Letter to the Editor

Diffraction-limited speckle-masking interferometry of the red supergiant VY CMa[*]

M. Wittkowski[1]**, N. Langer**[2]**, and G. Weigelt**[1]

[1] Max-Planck-Institut für Radioastronomie, Auf dem Hügel 69, D-53121 Bonn, Germany
[2] Institut für Physik, Universität Potsdam, D-14415 Potsdam, Germany

Abstract. We present the first diffraction-limited images of the mass-loss envelope of the red supergiant star VY CMa. The two-dimensional optical and NIR images were reconstructed from 3.6 m telescope speckle data using bispectrum speckle interferometry. At the wavelengths $\sim 0.8\,\mu$m (RG 780 filter), $1.28\,\mu$m, and $2.17\,\mu$m the diffraction-limited resolutions of 46 mas, 73 mas, and 124 mas were achieved. All images clearly show that the circumstellar envelope of VY CMa is non-spherical. The RG 780, $1.28\,\mu$m, and $2.17\,\mu$m FWHM Gauß fit diameters are 67 mas $\times$ 83 mas, 80 mas $\times$ 116 mas and 138 mas $\times$ 205 mas, respectively, or 100 AU $\times$ 125 AU, 120 AU $\times$ 174 AU and 207 AU $\times$ 308 AU (for a distance of 1500 pc). We discuss several interpretations for the asymmetric morphology. Combining recent results about the angular momentum evolution of red supergiants and their pulsational properties, we suggest that VY CMa is an immediate progenitor of IRC +10 420, a post red supergiant during its transformation into a Wolf-Rayet star.

1. Introduction

VY CMa (HD 58061, SAO 173591) is one of the most luminous red supergiants in the Galaxy with $L \simeq 4\,10^5\ L_\odot$ (Sopka et al. 1995, Jura & Kleinmann 1990) and is, therefore, an ideal candidate for the study of the progenitor phases of a supernova. Its distance is about 1500 pc, its spectral type is M5 Iae, and it is variable with a period of $\sim$2200 days (Jura & Kleinmann 1990; Malyuto et al. 1997; Danchi et al. 1994; Knapp & Morris 1985; Imai et al. 1997). Herbig (1972) found that VY CMa is embedded in an optical nebula with a size of $8'' \times 12''$ at 650 nm. The first high-resolution observations of the dust shell of VY CMa have been reported by McCarthy & Low (1975), McCarthy et al. (1977) and Danchi et al. (1994). VY CMa is a source of H_2O, OH and SiO maser emission (e.g. Masheder et al. 1974, Bowers et al. 1983, Bowers et al. 1993, Imai et al. 1997, Humphreys et al. 1997, Richards et al. 1998). The H_2O masers are distributed in an east-west direction, whereas OH masers are distributed in a north-south direction, possibly indicating a disk and a polar outflow. HST FOC images of the envelope of VY CMa were obtained by Kastner and Weintraub (1998). They show an asymmetric flux distribution in an approximately east-west direction with a brighter core of pure scattered light elongated from SE to NW.

In this *Letter* we present diffraction-limited $\sim 0.8\,\mu$m, $1.28\,\mu$m, and $2.17\,\mu$m bispectrum speckle interferometry observations of the mass-loss envelope of VY CMa. The observations are presented in Sect. 2, and the non-spherical shape of the envelope is discussed in Sect. 3. Clues for VY CMa's evolutionary state are derived in Sect. 4.

2. Observations

The optical and NIR speckle interferograms were obtained with the ESO 3.6 m telescope at La Silla on February 6,7 and 8, 1996. The optical speckle interferograms were recorded through the edge filter RG 780 (center wavelength of the filter/image intensifier combination: $\sim 0.8\,\mu$m; effective filter width: $\sim 0.07\,\mu$m) with our optical speckle camera described by Hofmann et al. (1995). The near infrared speckle interferograms were recorded with our NICMOS 3 camera through interference filters with center wavelength/FWHM bandwidth of $1.28\,\mu$m/$0.012\,\mu$m and $2.17\,\mu$m/$0.021\,\mu$m. The observational parameters (number of frames, exposure time per frame, pixel scale and seeing) are listed in Table 1. Diffraction-limited images were reconstructed from the speckle interferograms by the bispectrum speckle interferometry method (Weigelt 1977; Lohmann et al. 1983; Weigelt 1991). The power spectrum of VY CMa was determined with the speckle interferometry method (Labeyrie 1970). The atmospheric speckle transfer functions were derived from speckle interferograms of the unresolved stars H42071 (RG 780, 2000 frames), IRC 30098 ($1.28\,\mu$m, 600 frames) and 1 Pup ($2.17\,\mu$m, 800 frames).

Table 1. Observational parameters.

filter	number of frames	exposure time	pixel scale	seeing
RG 780	2000	60 ms	7.2 mas	$1\rlap{.}''5$
1.28 μm	800	150 ms	23.8 mas	$1\rlap{.}''0$
2.17 μm	800	100 ms	47.6 mas	$1\rlap{.}''5$

Table 2. VY CMa's parameters derived from the model fits to the visibility functions (one *two-dimensional* Gaussian flux distribution plus an unresolved object for the 1.28 μm and 2.17 μm observations and two *two-dimensional* Gaussian flux distributions for the RG 780 data). The parameters are the position angle of the major axis, the axes ratio (major/minor axis), the FWHM of major and minor axes, the azimuthally averaged FWHM diameter and the relative flux contributions of the Gaussian and the unresolved object. We estimate the errors of the position angles to $\sim \pm 10°$ and those of the FWHM sizes to $\sim \pm 15\%$.

data set	RG 780	1.28 μm	2.17 μm
PA ($°$) of the major axis	153/120	176	160
Axes ratio	1.2/1.1	1.5	1.5
Major axis (mas)	83/360	116	205
Minor axis (mas)	67/280	80	138
Average diameter (mas)	74/320	96	166
rel. flux of Gaussian	0.75/0.25	0.91	0.50
rel. flux of unres. comp.	0.00	0.09	0.50

Fig. 1 shows contour plots and intensity cuts of the reconstructed bispectrum speckle interferometry images of VY CMa. The resolutions of the 0.8 μm, 1.28 μm and 2.17 μm images are 46 mas, 70 mas and 111 mas, respectively. The envelope of VY CMa is asymmetric at each of the three wavelengths. The object parameters were determined by two-dimensional model fits to the visibility functions. The models consist of two-dimensional elliptical Gaussian flux distributions plus an additional unresolved component. The ~ 0.8 μm image is best described by two Gaussians while the 1.28 μm and the 2.17 μm images are best described by one Gaussian and an additional unresolved component. The best-fit parameters are listed in Table 2. We present the azimuthally averaged visibility function of VY CMa together with the corresponding azimuthally averaged two-dimensional fits in Fig. 2, in order to show the wavelength-dependent relative flux contribution of the unresolved component (dashed line).

3. Interpretation

Figs. 1 and 2 and Table 2 indicate that VY CMa consists of both an unresolved component and a resolved asymmetric extended component with an increasing average diameter at longer wavelengths. The unresolved component is probably the star itself or an additional compact circumstellar object. The relative intensity of this unresolved component decreases towards shorter wavelengths. The complete obscuration of the unresolved component close to the maximum of the stellar spectral energy distribution indicates a high optical depth of the circumstellar envelope, in agreement with the value from Le Sidaner and Le Bertre of $\tau_{10 \, \mu m} = 2.4$. The visibility functions, the images and the best fit parameters given in Table 2 at the three different wavelengths can be used as additional constraints in future two-dimensional radiation transfer modeling of the dust distribution. The resolved structures seen in Fig. 1 belong to the circumstellar envelope of VY CMa. In fact, the size of the image is of the order of the dust condensation radius R_c which has been estimated by Le Sidaner & Le Bertre within their spherically symmetric model to $R_c \simeq 12 R_\star$ with $R_\star \sim 4000 \, R_\odot$. They note, however, that their model fit to the spectral energy distribution of VY CMa is not entirely satisfactory and argue that the envelope of VY CMa may be non-spherical, as indicated by the high level of polarisation (Kruszewski & Coyne 1976). Danchi et al. (1994) found $R_c \simeq 5 R_\star$.

Several interpretations for the non-sphericity seen in all three images (Fig. 1) are possible. The position angle of the major axes of the approximately elliptical shapes is similar, although not identical for all three cases ($153°$ to $176°$; see Table 2).

This position angle is approximately perpendicular to the major axis of the H_2O maser distribution (Richards et al. 1998) and similar to the distribution of the OH masers (e.g. Masheder et al. 1974). Accordingly, we can interpret the structure of the circumstellar envelope of VY CMa as a bipolar outflow in a north-south direction caused by an obscuring equatorial disk in an east-west direction. The existence of an obscuring disk is supported by the obscuration of the central star at optical wavelengths. Such geometry was also discussed for IRC +10 216 by Weigelt et al. (1998) and Haniff & Buscher (1998) and has already been proposed for VY CMa due to maser observations by Richards et al. (1998).

Furthermore, we can not rule out that the unresolved component consists of an optically thick torus hiding a close binary, as was proposed for the Red Rectangle (e.g. Men'shchikov et al. 1998). This could lead to an asymmetric outflow in a north-south direction.

The mass-loss mechanism of VY CMa could also be erratic or stochastic, similar to the clumpy pulsation and dust-driven mass-loss events recently detected in the prototype carbon star IRC +10 216 (see Weigelt et al. 1998, Haniff & Buscher 1998). Although the reason for this anisotropy is unknown, and the physics of mass-loss in oxygen-rich red supergiants may differ from those in carbon-rich stars, the common properties of VY CMa and IRC +10 216 – both are pulsating cool luminous stars with extended convective envelopes – could result in similar mass-loss features. But individual clumps are not observable because of the larger distance of VY CMa, which leads to a regular asymmetric image elongated in a north-south direction.

Finally, our results are also conceivable with a more regular geometry of VY CMa's circumstellar envelope, for example, a disk-like envelope which appears elongated in a north-south direction due to the projection angle (discussed in Sect. 4 in more detail), which was proposed earlier for VY CMa on the basis of optical, infrared (Herbig 1970, 1972; McCarthy 1979; Efstathiou & Rowan-Robinson 1990), and maser observations
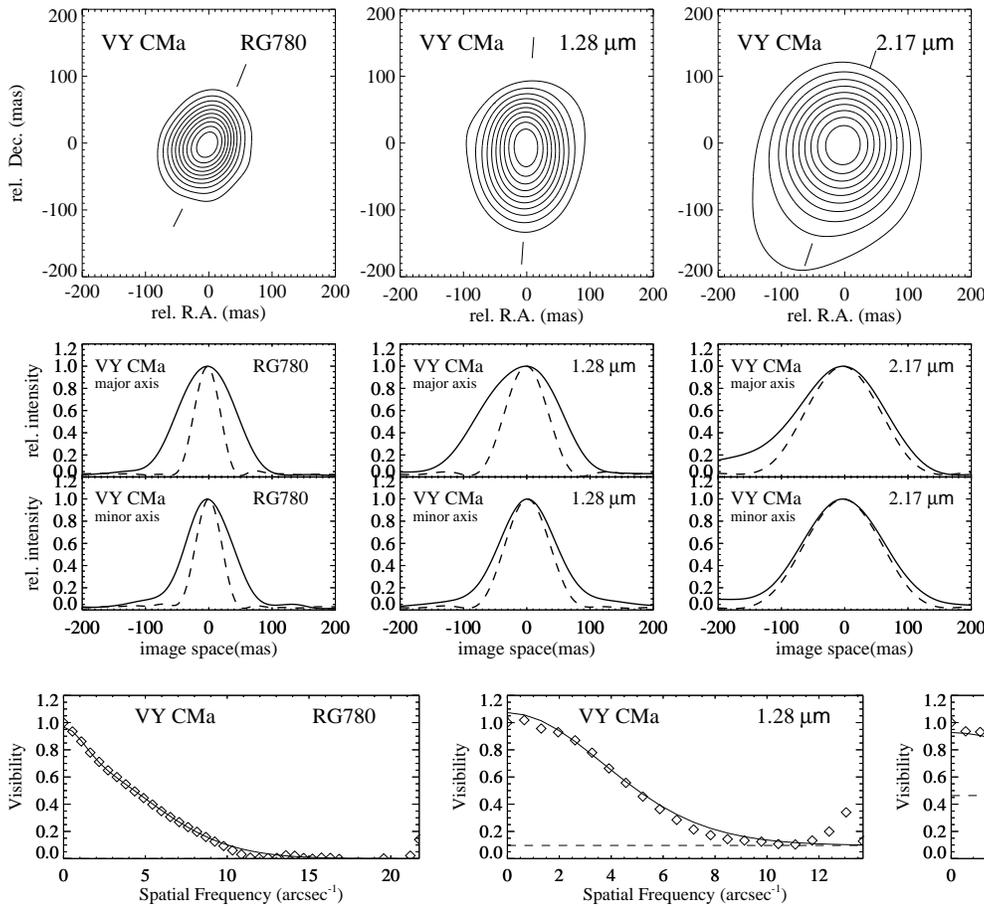
Fig. 1. *Top:* Contour plots of the RG 780 (*left*), 1.28 μm (*middle*) and 2.17 μm filter (*right*) bispectrum speckle interferometry reconstructions of VY CMa. The contours are plotted from 15% to 100% in 10 steps. North is at the top and east to the left. *Bottom:* Intensity cuts through the centers of the reconstructed images along the major and minor axes (solid lines). The position angles of these axes (RG 780: 153°, 1.28 μm: 176°, 2.17 μm: 160°) are taken from the two-dimensional fits to the visibility functions (see Table 2) and indicated in the contour plots. The dashed curves are cuts through the reconstructed images of the reference stars.

Fig. 2. Azimuthally averaged visibility functions of VY CMa and of the corresponding model flux distribution: (*left*) filter RG 780, (*middle*) 1.28 μm filter and (*right*) 2.17 μm filter. The diamonds indicate the observations, the solid line the azimuthally averaged fit curve of a two-dimensional Gaussian model flux distribution plus an unresolved object, and the dashed line the constant caused by just the unresolved component. The RG 780 visibility function is best described by two Gaussian flux distributions. For the fit parameters see Table 2. The visibility errors are ± 0.1 up to 80% of the telescope cut-off frequency and ± 0.2 for larger frequencies.

(van Blerkom 1978, Morris & Bowers 1980, Zhen-pu & Kaifu 1984).

4. Evolutionary status and conclusions

With a distance of ~ 1500 pc, the luminosity of VY CMa amounts to $\sim 4\,10^5\,L_\odot$ (see Jura & Kleinmann 1990). Fig. 3 compares this luminosity to a stellar evolutionary track of a $40\,M_\odot$ star in the HR diagram (see Langer 1991, for details of the computational method). It constrains the initial mass of VY CMa to the range $30...40\,M_\odot$, in agreement with e.g. Meynet et al. (1994), although models with rotation – which are not yet available for the post main sequence evolution at this mass – may lead to somewhat smaller values (cf. Heger et al. 1997). Accordingly, it is likely that VY CMa will transform into a Wolf-Rayet star during its further evolution. This is supported by the very high observed mass-loss rate of VY CMa of $\sim 10^{-4}\,M_\odot\,\mathrm{yr}^{-1}$ (Jura & Kleinmann 1990). In order to obtain a disk-like structure (see Sect. 3), the most likely mechanisms involve angular momentum. There is no indication of a binary companion to VY CMa, either from the spectrum of VY CMa

(Humphreys et al. 1972) or from high resolution imaging (see above). While this only excludes massive companions, it appears to be viable that the axial geometry is due to the star's rotation. Direct evidence for rotation being capable of producing a disk-like structure around red supergiants – possibly through the Bjorkman-Cassinelli-mechanism of wind compression (see Ignace et al. 1996) – comes from bipolar structures found in the AGB star V Hydrae (Stanek et al. 1995), for which rapid rotation ($v \sin i \simeq 13\,\mathrm{km\,s}^{-1}$) has been directly inferred from photospheric line broadening (Barnbaum et al. 1995).

According to Heger & Langer (1998), red supergiants drastically increase their surface rotation rate shortly before and during the evolution off the Hayashi line. Therefore, a disk-like envelope surrounding VY CMa may indicate that such a spin-up is currently in progress. As strong mass-loss from a convective star acts as a spin-down mechanism (Langer 1998, Heger & Langer 1998), a red supergiant must previously have lost the major part of its envelope for the competing spin-up process to dominate. This strongly supports the argument that the remaining mass of VY CMa's convective envelope is in fact small,
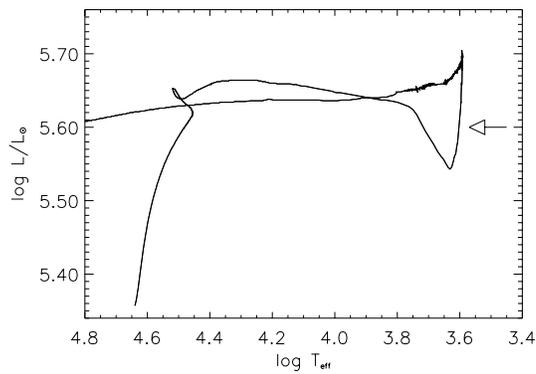
Fig. 3. Evolutionary track of a 40 $M_\odot$ star of solar metallicity, from the zero age main sequence to the red supergiant → Wolf-Rayet star transition. The luminosity of VY CMa is indicated by an arrow.

and that VY CMa is just about to leave the Hayashi line. It is also consistent with the very long observed pulsation period of VY CMa of about 6 yr according to the pulsational analysis of Heger et al. (1997), who showed that such large periods can be obtained in red supergiants for small envelope masses (cf. their Fig. 2a).

With this interpretation, VY CMa represents the immediate progenitor state of IRC +10 420, currently a mid A type supergiant evolving bluewards on human time scales on its way from the red supergiant stage to become a Wolf-Rayet star (Jones et al. 1993, Kastner & Weintraub 1995). A comparison with the 40 $M_\odot$ model shown in Fig. 3 predicts a current mass of VY CMa of 15 $M_\odot$ and a surface helium mass fraction of $Y \simeq 0.40$.

It is remarkable in the present context that bipolar outflows are observed in IRC +10 420 (Oudmaijer et al. 1994, 1996, Humphreys et al. 1997). A disk-like structure of VY CMa's envelope could be the basis for such flows, which occur when a fast wind originating from the star in a post-red supergiant stage interacts with a previously formed disk, according to hydrodynamic simulations of interacting wind flows (e.g., Mellema 1997, García-Segura et al. 1998).

References

Barnbaum, C., Morris, M. & Kahane, C., 1995, ApJ 450, 862
Bowers P.F., Johnston K.J., Spencer J.H. 1983, ApJ 274, 733
Bowers P.F., Claussen M.J., Johnston K.J., 1993, AJ 105,284
Danchi W.C., Bester M., Degiacomi C.G., Greenhill L.J., Townes C.H. 1994, AJ 107, 1469
Efstathiou A., Rowan-Robinson M. 1990, MNRAS 245, 275
García-Segura, G., Langer, N., Różyczka M., Franco J. 1998, ApJ, submitted
Haniff C.A., Buscher D.F., 1998, A&A 334, L5
Heger, A., Langer N., 1998, A&A 334, 210
Heger, A., Jeannin, L., Langer, N., Baraffe, I. 1997, A&A, 327, 224
Herbig G.H. 1970, ApJ 162, 557
Herbig G.H. 1972, ApJ 172, 375
Hofmann K.-H., Seggewiss W., Weigelt G. 1995, A&A 300, 403
Humphreys R.M., Strecker W.D., Ney E.P., 1972, ApJ 172, 75
Humphreys R.M., Smith N., Davidson K., et al. 1997, AJ 114, 2778
Ignace, R., Cassinelli, J. P. & Bjorkman, J. E. 1996, ApJ 459, 671
Imai H. et al. 1997, A&A 317, L67
Jones T.J., Humphreys R.M., Gehrz R.D., et al., 1993, ApJ 411, 323
Jura M., Kleinmann S.G. 1990, ApJS 73, 769
Kastner J.H., Weintraub D.A., 1995, ApJ 452, 833
Kastner J.H., Weintraub D.A., 1998, AJ 115, 1592
Knapp G.R., Morris M. 1985, ApJ 292, 640
Kruszewski A., Coyne G.V. 1976, AJ 81, 641
Labeyrie A., 1970, A&A 6, 85
Langer N. 1991, A&A 252, 669
Langer N. 1998, A&A 329, 551
Le Sidaner P., Le Bertre T., 1996, A&A 314, 896
Lohmann A.W., Weigelt G., Wirnitzer B. 1983, Appl. Opt. 22, 4028
Malyuto V., Oestreicher M., Schmidt-Kaler T. 1997, MNRAS 286, 500
Masheder M.R.W., Booth R.S., Davies R.D., 1974, MNRAS 166, 561
McCarthy D.W. 1979, in IAU-Colloq. No. 50 on *High Angular Resolution Stellar Interferometry*, ed. J. Davis et al., p. 18-1
McCarthy D.W., Low F.J. 1975, ApJ 202, L37
McCarthy D.W., Low F.J., Howell R.R. 1977, ApJ 214, L85
Men'shchikov A.B., Balega Y.Y., Osterbart R., Weigelt G., 1998, New Astronomy 3, 601
Meynet, G., Maeder, A., Schaller, G., Schaerer, D., Charbonnel, C. 1994, A&AS, 103, 97
Mellema, G. 1997, A&A 321, L29
Morris M., Bowers P.F. 1980, AJ, 85, 724
Oudmaijer, R.D., Geballe, T.R., Waters, L.B.F.M., Sahu, K.C. 1994, A&A, 281, L33
Oudmaijer, Groenewegen M.A.T., Matthews H.E., Blommaert J.A.D.L., Sahu K.C. 1996, MNRAS 280, 1062
Richards A.M.S., Yates J.A., Cohen R.J., 1998, MNRAS 299, 319
Sopka R.J., Hildebrand R., Jaffe D.J., et al., 1985, ApJ 294, 242
Stanek K., Knapp G., Young K., Phillips T. 1995, ApJS 100, 169
van Blerkom D., 1978, ApJ 223, 835
Weigelt G.P. 1977, Opt. Comm. 21,55
Weigelt G. 1991, in Progress in Optics (ed. E. Wolf) 1991, p. 293
Weigelt G., Balega Y., Blöcker T., Fleischer A.J., Osterbart R., Winters J.M., 1998, A&A 333, L51
Zehn-pu Z., Kaifu N., 1984, A&A 138, 359